Soil Dynamics and Earthquake Engineering 31 (2011) 106–118

Contents lists available at ScienceDirect

Soil Dynamics and Earthquake Engineering

journal homepage: www.elsevier.com/locate/soildyn

Earthquake early warning: Concepts, methods and physical grounds

Claudio Satriano [a,c,*], Yih-Min Wu [b], Aldo Zollo [c], Hiroo Kanamori [d]

[a] RISSC-Lab, AMRA scarl, Naples, Italy
[b] Department of Geosciences, National Taiwan University, Taipei 10617, Taiwan
[c] Department of Physics, University of Naples Federico II, Naples, Italy
[d] Seismological Laboratory California Institute of Technology, USA

ARTICLE INFO

Article history:
Received 22 October 2009
Received in revised form
10 July 2010
Accepted 20 July 2010

ABSTRACT

Modern technology allows real-time seismic monitoring facilities to evolve into earthquake early warning (EEW) systems, capable of reducing deaths, injuries, and economic losses, as well as of speeding up rescue response and damage recovery. The objective of an EEW system is to estimate in a fast and reliable way the earthquake's damage potential, before the strong shaking hits a given target.

The necessary framework for EEW implementation is provided by the observed relationships between different parameters measured on the signal onsets and the final earthquake size. The implication of these observations on the physics of fracture processes has given rise to a significant debate in the seismological community.

Currently, EEW systems are implemented or under testing in many countries of the world, and different methodologies and procedures have been studied and developed. The leading experience of countries like Japan or Mexico shows that, with a proper education of population and end-users, and with the design of real-time systems for the reduction of vulnerability/exposure, EEW can be an effective approach to the mitigation of the seismic risk at short time-scales.

1. Introduction

Earthquakes are among the most damaging events caused by the Earth itself. As urbanization progresses worldwide, earthquakes pose serious threat to lives and properties for urban areas near major active faults on land or subduction zones offshore.

The mitigation of the seismic risk is a complex task, which requires the cooperation of scientists, engineers and decision makers, and that has to be approached at different time scales ([1,2]; Fig. 1). These range from *years*, where long-term forecast and scenarios should drive the improvement of urban planning and building codes, to *months* or *weeks*, when anomalous seismicity patterns can rise the level of alertness in a certain area, down to the short term (*days* to *hours*), where the availability of reliable predictions of size, location and time of an incoming earthquake would be required.

However, the processes of earthquake preparation and generation are extremely complex and our observations cover a relatively short period compared to large earthquake cycles. As a result of this, reliable earthquake prediction is not currently possible [3,4]. Even if such predictions were available, it is desirable to implement measures to protect large urban areas from damages and losses.

For this reason a new approach to the short-term risk mitigation has emerged in the last two decades, based on the advent of digital seismology, and on the advances in communications and automatic processing. This new paradigm is founded on the concept of *real-time earthquake information systems* [5], namely networks of computerized seismic stations that integrate rapid telemetry and automatic processing, in order to provide fast and reliable information on earthquake parameters (location, time and size) and on the expected ground motion, supporting and improving the emergency response. Thanks to continuous theoretical and computational improvements, the reporting time of these systems has evolved from a few minutes to a few seconds after the earthquake occurrence, making it possible, in certain conditions, to provide earthquake information before the ground shaking has actually reached a certain target.

This procedure is known as *earthquake early warning* (EEW) and is today becoming one of the practical and promising approaches to reduce the loss caused by large earthquakes [1,6–11].

2. The concept of early warning

The term "early warning" was born during the cold war for describing a military strategy to prevent the potential threat from

* Corresponding author. Now at: Institute de Physique du Globe de Paris, 4 Place Jussieu, 75252 Paris Cedex 05, France. Tel.: +33 1 44272468.
E-mail address: satriano@ipgp.fr (C. Satriano).

0267-7261/$ - see front matter © 2010 Elsevier Ltd. All rights reserved.
doi:10.1016/j.soildyn.2010.07.007

ballistic intercontinental missiles. These early warning systems (still operational) were designed to alert target areas as soon as a missile was detected by a radar setup or a launch discovered by a satellite system. In this context the term "lead-time" was defined as the time that has elapsed since the detection of the missile and the estimated impact on the target.

In the last decades the use of the term "early warning" has broadened to include various types of risks, though with differences in its application. Today early warning systems are designed for epidemiological, economical, social, and for all the types of natural and environmental risks. In many contexts, like for hydro-geological and volcanic risk, the warning is not based on the rapid detection of the ongoing event, but on the recognition of some precursory phenomena that can trigger a potentially dangerous event (like intensive rainfall for hydrological risk, or earthquakes and ground deformation for volcanic risk). In this kind of approaches the lead-time is generally larger, but the probability of issuing false alarms can be significant.

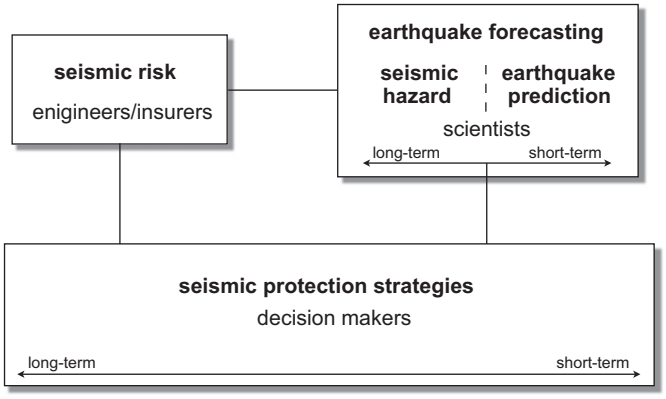

Fig. 1. Mitigation of seismic risk can be performed at several time scales, from the long-term (decades) to the short term (minutes to seconds). Different experts are required in this task (redrawn from [2]).

3. Earthquake early warning systems: regional and onsite approach

Earthquake early warning is similar in concept to the missile early warning, since it is based on the rapid detection of a seismic event after its occurrence.

The first idea of a system which is able to provide an early alert for incoming ground shaking dates back to 1868 (well before the origin of the "Early Warning" term and of its first, military implementation) and was proposed by Cooper [12] in an editorial in the San Francisco Daily Evening Bulletin.

Cooper's idea (which was never implemented) was based on a key concept that is behind several modern EEW systems: information (which travels at the speed of an electromagnetic signal—about 300,000 km/s) is much faster than seismic waves (which travel at speeds of the order of a few km/s). Therefore, if a rapid detection system is placed next to a seismogenic zone, an alarm can be sent to a distant region before the seismic waves will hit the target. This concept is the basis of the so called *regional* (or *front-detection*, or *network-based*) EEW systems, where data from a seismic network next to the epicentral area is used to rapidly detect and locate an earthquake, determine its magnitude and predict the ground motion at a specified target, using "*a priori*" known, ground motion prediction equations.

A second, important fact behind EEW is that most of the radiated energy is carried by the slower-traveling phases (*S*- and surface waves, traveling at about 3.5 km/s or less), which arrive at any location with a delay after small-amplitude, higher-velocity *P*-waves (traveling at about 6–7 km/s).

For this reason, the maximum, theoretical lead-time for regional EEW systems is often defined as the time difference between the *S* arrival at the target and the first *P* arrival at the seismic network. However an EEW system typically requires a few seconds to detect the event, evaluate its severity, and decide whether to issue an alarm. This time has to be subtracted from the theoretical lead-time, so that the effective lead-time is always smaller (Fig. 2). It is clear that, for such systems, the lead-time increases with the distance of the target and with the rapidity of

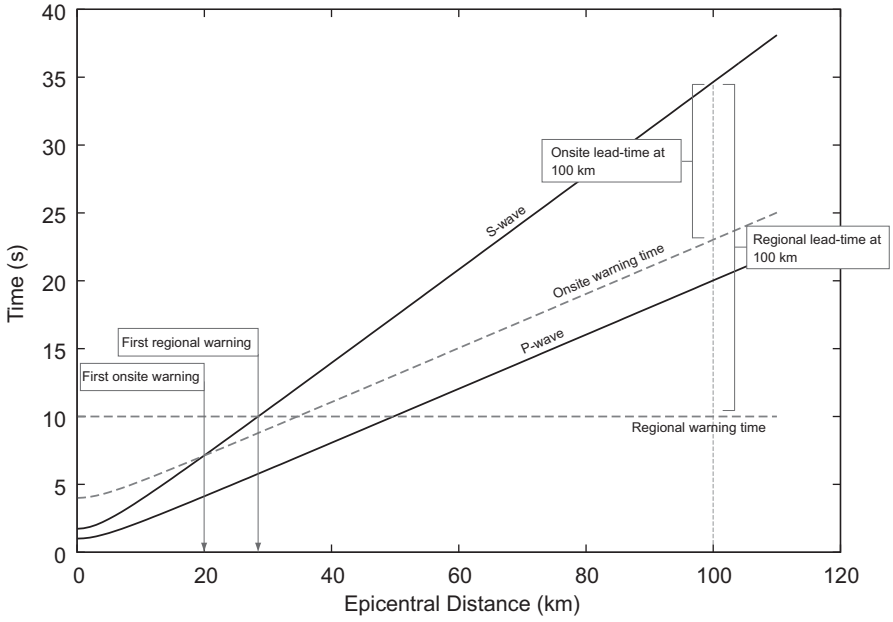

Fig. 2. Comparison of warning times and lead-times for onsite and regional EEW approaches. The onsite warning time depends on the *P* arrival time at the site and on a (generally) fixed analysis window (here set to 3 s). The regional warning time depends on the source-network geometry and on the algorithms employed and is generally of the order of a few seconds (e.g. 10 s). An onsite system can provide a warning to targets closer to the epicenter. However, when a regional approach is possible, the associated lead-time quickly becomes larger than the onsite lead-time.

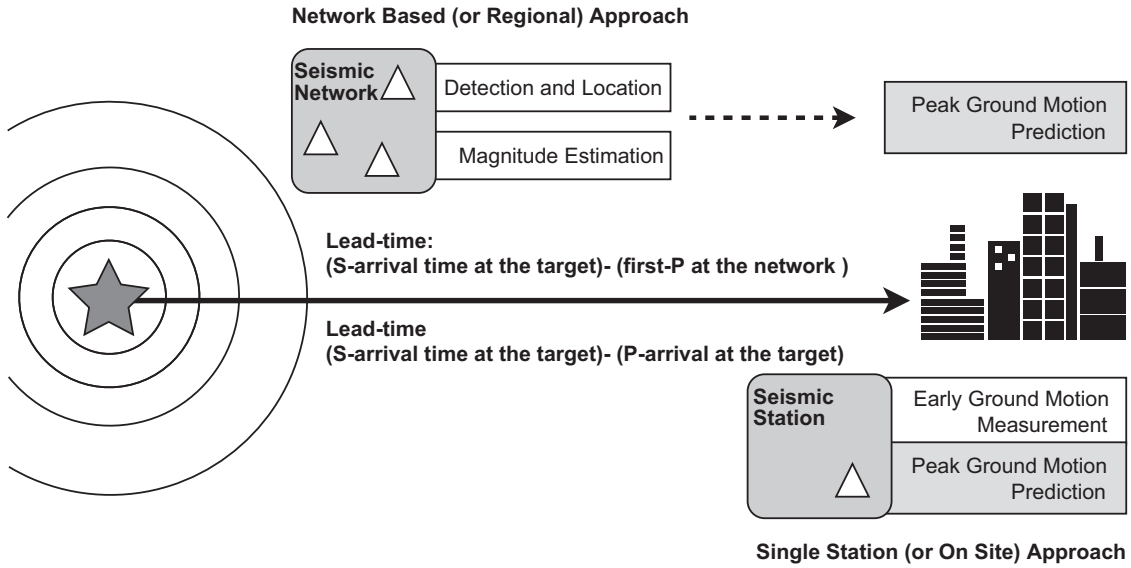

Fig. 3. The two possible approaches to earthquake early warning share a common objective: to predict the ground shaking at a given target. See also Table 1.

Table 1
Comparative table of the regional and the onsite approaches to earthquake early warning. The regional approach is the most comprehensive, since it leverages the information from a seismic network deployed next to the epicenter to evaluate the earthquake parameters and predict the regional ground motion. The onsite approach is faster, since it is based on a local measurement of earthquake ground motion, and can provide useful early warning at sites at short distances from the epicenter, where an early warning is often most needed. This can however be done at the price of a lower accuracy on the estimation of earthquake parameters.

	Regional	**Onsite**
Network deployment	Source region	Target area
Data analysis	Network based	Single station
Output parameters	Location, magnitude	Location, magnitude or expected intensity
Accuracy on source parameter estimation	Good to high	Moderate
Lead-time	Ts at the target–Tp at the source	Ts at the target–Tp at the target

the detection. On the other hand, if the target site is close to the epicentral area, the regional approach is not viable, since the lead-time can be too small for any application, or even null.

An alternative approach is the *onsite warning*, where one or more seismic sensors are placed directly at the target, and the beginning part of the ground motion (mainly *P* wave) observed at the site is used to predict the ensuing ground motion (mainly *S* and surface waves) at the same site. In this case, the theoretical lead-time can be defined as the time interval between the *P* and the *S* arrival at the target, though, again, some seconds for detection and computation must be taken into account. Similar to the case for the regional approach, the lead-time for the onsite methodology increases with the epicentral distance, due to the growing travel-time difference between the slower *S*-phase and the faster *P*-phase. An onsite EEW system can provide a useful lead-time where a regional EEW system cannot; however, when a regional strategy is possible, it generally provides a larger lead-time (Fig. 2).

A comparison between regional and onsite EEW systems is given in Fig. 3 and Table 1.

4. Time and accuracy: the challenge of an earthquake early warning system

The key parameter of any early warning system is time. The larger the time available before the catastrophic phenomenon hits the target, the more effective and comprehensive will be the countermeasures that can be taken.

As illustrated in Fig. 2, the lead-time for EEW applications is of the order of a few seconds to a few tens of seconds depending on the target epicentral distance. Setting up a risk mitigation strategy on such short time scales is still feasible. Even a few seconds of lead-time can be enough for pre-programmed emergency measures for critical infrastructures (deceleration of rapid-transit vehicles and high-speed trains, orderly shutoff of gas pipelines to minimize fire hazards), facilities (controlled shutdown of high-technological manufacturing operations, safe-guarding of critical computers and data centers, bringing elevators to a stop at the nearest floor), or at personal level (hospitals and surgeons can suspend or adjust delicate and critical operations, workers can move away from hazardous positions, students can shelter under their desks).

There is always a trade-off between the warning time and the reliability of the earthquake information. The more data acquired after the event occurrence, the more accurate will be the warning and the lower is the probability of false alarms. However, of course, the lead-time will be shorter. Generally, an information updating procedure is necessary for any EEW system.

On the other hand, EEW applications need to be carefully tailored on the basis of the required lead-time, the intensity of the action and their false-alarm acceptability: a critical action, which requires a low probability of false alarms, will have a smaller lead-time, compared to low-impact actions, since additional validation is required to the EEW system [13,14].

5. Earthquake early warning systems worldwide

Allen et al. [11] provide a thorough review of the status of EEW around the world, describing the operating principles and the rate of success of each system. Here we will just report that the countries where EEW systems have been operative for some time are Mexico [15,16], Japan [17,18], Taiwan [19–21], Romania [22,23] and Turkey [24–26]. Other countries are actively experimenting and prototyping their systems, like ElarmS in California [27–29], Virtual Seismologist in California and Switzerland [30] and PRESTo in Southern Italy ([31,38]).

It is interesting to mention that commercial implementations of the EEW principles have started to appear. One is the "Home seismometer", developed and commercialized in Japan. It is a box that incorporates an accelerometer and that can receive messages from the Japanese public EEW system to provide both onsite and regional warning functions [86].

6. Principles and methodologies of earthquake early warning

The objective of an EEW system is to estimate in a fast and reliable way the earthquake's damage potential, before the strong shaking hits the target.

For regional EEW systems, this goal is accomplished following the classical model proposed by Heaton [5], which comprises 4 steps:

1. *Event detection and location*: A conceptually simple problem: many systems just use standard methodologies developed for non-real-time networks; other approaches are specifically designed for real-time operations and can provide faster hypocentral determinations. In general high-precision results are achievable.
2. *Magnitude estimation*: A conceptually difficult problem: to be fast, magnitude has to be estimated from the first few seconds of recorded signal, this implies the development of empirical regressions between quantities measured on the early portion of the seismogram and the final magnitude. This often leads to a low accuracy in the determinations.
3. *Peak ground motion prediction at the target site*: A well-established problem, critically dependent on accuracy of the attenuation law. Simplified assumptions about the source and propagation models are often required.
4. *Alert notification*: Crucially depends on uncertainties related to source parameter and peak ground motion estimations. It must be designed according to the target application, and should include a probabilistic evaluation of missed/false alarms.

In contrast to the regional approach to EEW, the onsite technique is generally more straightforward, since it aims at estimating the expected ground shaking, associated to *S* or surface waves, directly from the recorded shaking, associated to the early *P* signal. This is again accomplished through the use of empirical regressions between measurements performed in the first few seconds and the final peak ground motion. Nevertheless, as we will see, there are certain onsite approaches that evaluate location (or hypocentral distance) and magnitude. They are sometimes used as support for regional EEW systems, in order to reduce lead-times and extend the region of applicability.

In the following we will review the principles and the methodologies employed for estimating earthquake source parameters and/or ground shaking intensities for both the approaches to EEW.

6.1. Earthquake location

Among the regional EEW systems, we can distinguish between the techniques for earthquake detection and location based on standard procedures and those that include the additional information of current clock time (t_{now}), to improve the constraint on the location at an earlier time and with fewer observations than for standard earthquake location.

The ElarmS approach [28] belongs to the first class. An event is declared when a *P* wave is detected at the first station by a waveform processing system. ElarmS employs an STA/LTA (short-term-average/long-term-average) picker [32], using 5 s for the LTA and 0.5 s for the STA. The initial hypocenter is placed beneath the first triggering station at a fixed depth, which depends on the regional tectonics; with two triggers the epicenter is placed between the two stations, and the depth is still fixed; with three or more triggers, event location and origin time are estimated using a grid search algorithm.

Although based on simple concepts the ElarmS approach clearly evidences that the problem of earthquake location for regional EEW is *inherently time-dependent*, since the quantity of available information (the number of triggers) increases with time.

Rydelek and Pujol [33], and Horiuchi et al. [34] introduced the idea of considering stations not yet triggered at the current clock time (t_{now}) as an additional piece of information, which can further constrain the hypocentral position.

This principle can be quite easily illustrated by the methodology of Rydelek and Pujol, who constrain the epicentral location using only two stations (Fig. 4). Let us consider a seismic network and an earthquake occurring somewhere within or next to the network, at an arbitrary time. The seismic waves generated by the earthquake will propagate through the network, eventually reaching all the stations. However, we can assume that there will be a moment when only two stations, namely 1 and 2, placed at distances d_1 and d_2 from the epicenter, have detected the first *P* arrival, at times t_1 and t_2, respectively. Assuming a homogeneous model with *P*-wave velocity *V*, the following relation holds:

$$t_2 - t_1 = \frac{1}{V}(d_2(\mathbf{x}) - d_1(\mathbf{x})) = tt_2(\mathbf{x}) - tt_1(\mathbf{x}) \quad (1)$$

where $\mathbf{x}$ is the vector of epicentral coordinates and $tt = d/V$ is the travel-time of the *P*-wave from the epicenter to the station. Eq. (1) defines a hyperbola, where the epicenter must lie. This is not a strong constraint, since hyperbola is an open curve; however the fact that other stations have not yet triggered provides further limits. For instance, if station 3 has not yet recorded the *P* arrival, then its distance d_3 from the epicenter has to be greater than d_1 and d_2:

$$\frac{1}{V}(d_3(\mathbf{x}) - d_i(\mathbf{x})) = tt_3(\mathbf{x}) - tt_i(\mathbf{x}) \geq 0, \quad i = 1,2 \quad (2)$$

The same inequalities as (2) hold for all the other not-triggered stations. The possible epicentral locations are limited by the inequalities (2) to a segment along the hyperbola, which can provide a rather accurate solution, depending on the station geometry and on the actual position of the hypocenter.

Horiuchi et al. [34] extended the approach by Rydelek and Pujol [33], considering that, as time passes since the first two triggers: (a) the constraint on the earthquake location given by Eq. (2) increases and (b) other stations will trigger, further improving the location. Eq. (2) can be generalized to:

$$tt_j(\mathbf{x}) - tt_i(\mathbf{x}) \geq t_{now} - t_i \quad (3)$$

where *i* is a triggered station and *j* a not-yet-triggered station. This inequality identifies a volume in the space, where the hypocenter must be, which is smaller as time passes by and, thus, t_{now}

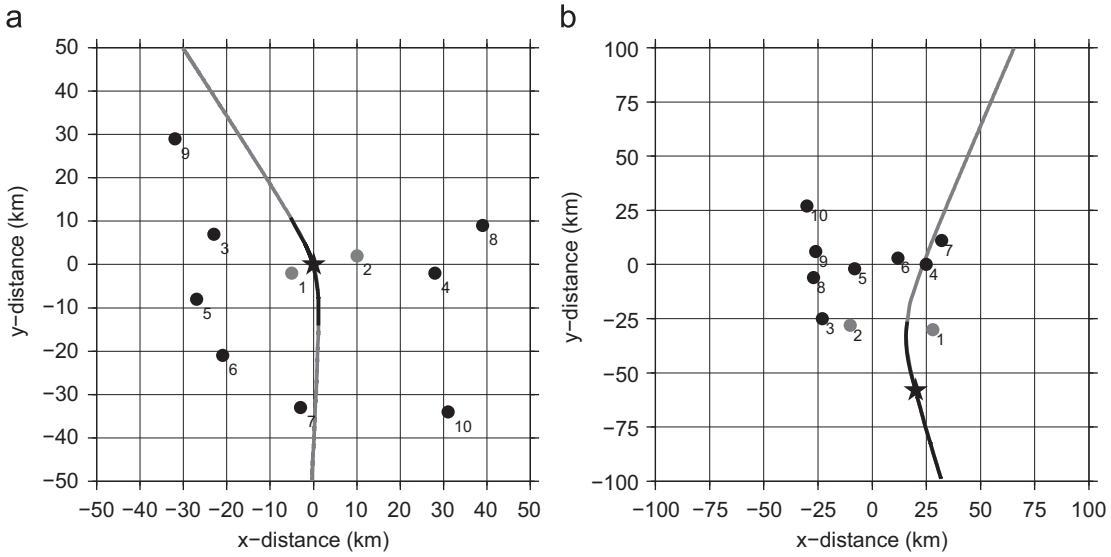

Fig. 4. The technique of Rydelek and Pujol [33] for determining the epicentral position with just two triggered stations. (a) A network of seismic stations (1–10) is located randomly in a certain area. An earthquake occurs, and generates *P* waves that will eventually be recorded by all stations, which have been labeled according to the order of *P* arrivals. The first arrivals at stations 1 and 2 can be used to construct a hyperbola (grey curve) on which the epicenter of the earthquake must lie. The black segment of the hyperbola comes from the constraint that the other stations did not record the two first arrivals. (b) In this case, the earthquake lies outside of the array. The epicentral location on the outward segment of the hyperbola in not constrained, and therefore at least three stations would be needed to locate this event. The hyperbolic segment away from the array may be used to constrain the azimuth of the event.

increases. Eq. (2) is a special case of (3) at the time $t_{now}=t_i$ when station i is triggered.

Cua and Heaton [30] integrated the approaches described by Horiuchi et al. [34] and Rydelek and Pujol [33] with the concept of Voronoi cells, in order to start the location with one single triggering station. A Voronoi cell associated to a given station is the set of all the possible location coordinates that are *closer in time* to that station. The epicentral location is initially constrained by the Voronoi cell associated to the first triggering station. At any time t_{now} after the first trigger, the hypocentral solution is given by the intersection of the Voronoi cell and the volume defined by Eq. (3).

Satriano et al. [35] further extended the above ideas by (a) introducing equal differential time (EDT) surfaces [36] and volumes, which incorporate and generalize the concepts of Voronoi cells and hyperbolas; (b) defining the hypocentral location as a probability density function; and (c) applying a full non-linear global search for each update of the location estimate.

Rosenberger [37] has recently proposed a methodology for rapid epicentral location from the arrival time order, based on generalized Voronoi diagrams and that does not require any velocity model.

Among the onsite EEW methods, the UrEDAS system [39] is able to estimate the earthquake location from a single station. In this approach, the magnitude is first determined on the basis of the predominant period of *P*-waves (see Section 6.2), then the hypocentral distance is inferred from the peak *P*-wave amplitude by using an empirical magnitude–amplitude relation that includes the hypocentral distance as a parameter. Finally, the earthquake location can be determined by combining the distance with the direction of *P*-wave particle motion.

Odaka et al. [17] introduced a slightly different method for fast estimation of the epicentral distance from a single seismic record. They observed that the initial part of the envelope of the vertical acceleration waveform can fit a function of the form of $Bt\exp(-At)$. The parameter B defines the slope of the initial part of the *P* waves, and A is related to the amplitude variation with time. They evaluated the parameters A and B, fitting the first 3 s of waveform envelope for several Japanese earthquakes, with magnitudes ranging from 3.9 to 7.3, and observed that $\log B$ is proportional to $-\log d$, where d is the epicentral distance. By determining the best-fit values for parameters A and B on the first seconds of the envelope of the vertical acceleration, it is therefore possible to rapidly determine the epicentral distance. Reciprocally to the UrEDAS approach, this methodology also provides fast magnitude estimation, measuring the maximum *P*-wave amplitude in a short time window and using a similar magnitude–amplitude relation, which depends on the epicentral distance.

6.2. Magnitude estimation

Rapid magnitude estimation for EEW is based on the observation, made by several authors, that quantities like the peak displacement, or the characteristic period, measured in the first few seconds of the recorded *P*- or *S*-signal, can be correlated to the final earthquake size. These empirical observations have opened many debates about the physics of the earthquake rupture initiation. Two are the basic questions: How do early *P*- and *S*-signals carry information on the final earthquake size? And, how is it possible to estimate the earthquake size while the rupture (or the seismic radiation) is still ongoing?

In the following we will overview the empirical relationships between early-measured parameters and the earthquake size, and we will describe how they are used for real-time magnitude estimation. The physical implications of the observed correlations are discussed in Section 6.3.

Among the possible parameters measurable in real-time, which are empirically related to the earthquake magnitude, the characteristic period and peak displacement amplitude of initial *P*-waves have so far proved to be the most robust, and are used in most of the worldwide EEW systems.

Nakamura [39,40], with the onsite UrEDAS system, pioneered the idea of using the initial portion of the recorded *P*-waves for magnitude determination. The method of Nakamura, which has been implemented also in the regional ElarmS system [27], consist in using the predominant period (or frequency) from the initial 2–4 s of *P* waves to determine the magnitude. The predominant period (called τ_p by Allen and Kanamori [27]) is computed continually in real time from vertical component of

velocity (v) and acceleration (a) signals at each station (recorded at two separate sensors or computed by differentiation or integration from a single velocimeter or accelerometer), and it is defined through the recursive relation

$$\tau_{p,i} = 2\pi\sqrt{\frac{V_i}{A_i}} \tag{4}$$

where

$$V_i = \alpha V_{i-1} + v_i^2$$

$$A_i = \alpha A_{i-1} + a_i^2$$

and α is a smoothing constant with values between 0 and 1. Nakamura [39,40] and Allen and Kanamori [27] observed that the logarithm of the predominant period τ_p, measured within 2–4 s from the first P arrival, linearly scales with the earthquake size. The resulting regression law can be used to quickly determine the magnitude.

Kanamori [9] proposed another period parameter, called τ_c, similar to τ_p, but calculated in a slightly modified way. The ground-motion filtered displacement, $u(t)$, and velocity, $\dot{u}(t)$, from the vertical component record are used to compute a ratio r, defined as

$$r = \frac{\int_0^{\tau_0} \dot{u}^2(t)\,dt}{\int_0^{\tau_0} u^2(t)\,dt} \tag{5}$$

where the integration is taken over the *fixed* time interval $(0, \tau_0)$, after the onset of P wave. In a series of studies [41–46], τ_0 is set to 3 s. Displacement signals are obtained by integration and are high-pass filtered at 0.075 Hz (Butterworth with 2 order of pole) to remove long period drifts. Using the Parseval's theorem, we have that

$$r = \frac{4\pi^2 \int_0^{\infty} f^2 |\hat{u}(f)|^2\,df}{\int_0^{\infty} |\hat{u}(f)|^2\,df} = 4\pi^2 \langle f^2 \rangle \tag{6}$$

where $\hat{u}(f)$ is the frequency spectrum of $u(t)$, and $\langle f^2 \rangle$ is the average of f^2 weighted by $|\hat{u}(f)|^2$. Thus,

$$\tau_c = \frac{1}{\sqrt{\langle f^2 \rangle}} = \frac{2\pi}{\sqrt{r}} \tag{7}$$

can be used as a parameter representing the average period of the initial portion of the P wave. τ_c approximately represents the P wave pulse width, which increases with the earthquake size and can be used to estimate the magnitude.

Cua and Heaton [30], in their Virtual Seismologist (VS) approach, also use a measure of the relative frequency content of ground motion to determine earthquake magnitude. Their quantity is defined from the ratio of peak vertical acceleration over peak vertical filtered displacement, measured on the P signal available at a given time. The information is combined at each time step using a Bayesian framework.

The effectiveness of using the early frequency content to estimate the final earthquake magnitude has been debated in literature. Wu and Kanamori [41] show a linear trend between τ_c and M_w for 54 events with at least 4 measurements from Japan, Taiwan, and southern California records, in the magnitude range $4.0 < M < 8.5$ (Fig. 5, left); Rydelek and Horiuchi [47], on the other hand, from the analysis of 52 events with $6.0 \le M \le 8.0$ recorded by the Hi-Net array in Japan, claim that there is no significant correlation between τ_p and the earthquake size in this magnitude range (Fig. 5, right). From a numerical study, conducted on synthetic seismograms, Yamada and Ide [48], conclude, among the other things, that the linear relationship between the τ_p parameter and the final magnitude has an upper limit that is controlled by the length of the time window employed for the measurement.

Wu and Zhao [49] and Zollo et al. [50] investigated a different kind of parameter: the peak displacement amplitude, measured on the early P (and S) phases.

Wu and Zhao [49] called this parameter P_d and defined it as the peak displacement measured on the vertical component, using a three seconds window after the P arrival. They studied the attenuation of P_d with the hypocentral distance R in southern California, using a relationship that depends on the magnitude M:

$$\log P_d = A + BM + C\log R \tag{8}$$

where A, B and C are constants to be determined from a regression analysis. For a regional warning approach, when an earthquake location (and thus the hypocentral distance R) is determined by the

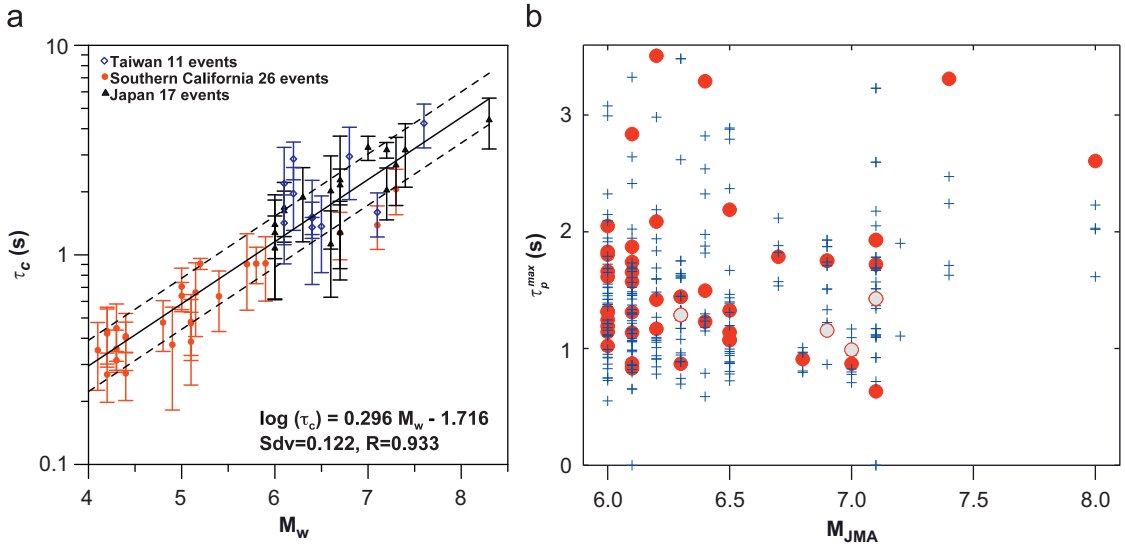

Fig. 5. (Left) Estimates of the τ_c parameter using the nearest stations for 54 events recorded in Japan (black triangles), southern California (red solid circles) and Taiwan (blue diamonds) (from [44]). Symbols show the event-average with standard deviation. Solid line shows the least squares fit and the two dashed lines show the range of one standard deviation. (Right) Plot of the τ_p parameter vs. magnitude for large earthquakes ($M > 6.0$) recorded by the Hi-Net seismic array in Japan (from [47]). Circles show the mean values of τ_p, estimated from the five stations (cross symbols) that were closest to the epicenter of each earthquake. (For interpretation of the references to colour in this figure legend, the reader is referred to the web version of this article.)

P-wave arrival times at stations close to the epicenter, this relationship can be used to estimate the earthquake magnitude. Wu and Zhao show that, for earthquakes in southern California, the P_d magnitudes agree with the catalog magnitudes with a standard deviation of 0.18, for events with magnitude less than 6.5.

Zollo et al. [50] independently introduced a peak amplitude quantity that is similar to the P_d of Wu and Zhao [49], though with two relevant differences: (a) the time window is not fixed to 3 s—the peak displacement scaling is instead investigated on increasing time windows; (b) the initial *S*-phases are also considered. They observed in fact that, in a regional EEW approach, where a dense array is deployed in the epicentral area, the initial *S*-phases are available at the stations close to the epicenter before the strong ground shaking reaches a distant target. Therefore *S*-wave information can be used to improve the magnitude estimation.

Zollo et al., make use of Eq. (8) to normalize the observed P_d to a reference distance of 10 km and then investigate the distance-independent relationship:

$$\log P_d^{10\,\mathrm{km}} = A' + B'M \tag{9}$$

They studied 376 three-components strong-motion traces of moderate-to-large European earthquakes, recorded within 50 km from the epicenter, and retrieved regression laws for time windows of 2 s of *P*-wave (2*P*), and 1 and 2 s of *S*-wave (1*S* and 2*S*). They conclude that it is possible to use Eq. (9) to estimate earthquake magnitude, using both early *P* waves and *S*-waves recorded at the closest stations.

Rydelek et al. [51], using a data-set of Japanese earthquakes, questioned that the relationship between $\log P_d$, measured on a time window of 2 s, and the final magnitude is linear only up to magnitude 5.5. After that it starts exhibiting a *saturation effect* (Fig. 6, top).

Zollo et al. [52] and Lancieri and Zollo [53], by studying a set of 256 shallow crustal events of moderate-to-large magnitude recorded in Japan, observed that, for time windows of 4*P*, 1*S* and 2*S*, the linear relation (9) holds over the entire magnitude range, with coefficients similar to those obtained by Zollo et al. [50], and that only when considering a 2*P* time window, the retrieved scaling shows the saturation effect (Fig. 6, bottom). A possible explanation of this effect is discussed in the next section.

Odaka et al. [17], in their onsite approach, also use the peak *P* displacement and the epicentral distance, determined from a single station, to estimate the magnitude, using a relation similar to Eq. (8).

Iervolino et al. [13] and Cua and Heaton [30] independently introduced a probabilistic formulation for the magnitude estimate, through the Bayes' theorem:

$$f_{M|\mathbf{d}}(m|\mathbf{d}) = \frac{f_{\mathbf{d}|M}(\mathbf{d}|m) f_M(m)}{\int_{M_{min}}^{M_{max}} f_{\mathbf{d}|M}(\mathbf{d}|m) f_M(m)\, dm}$$

where $f_{M|\mathbf{d}}(m|\mathbf{d})$ is the conditional probability density function (PDF) of magnitude M given the data vector $\mathbf{d}$ of measurements of a certain magnitude-related parameter (e.g. τ_c, τ_p, or P_d), $f_{\mathbf{d}|M}(\mathbf{d}|m)$ is the conditional PDF of data $\mathbf{d}$, given the magnitude M, and $f_M(m)$ is the *a priori* knowledge on the magnitude distribution. Iervolino et al. set $f_M(m)$ to the Gutenberg–Richter recurrence relationship (G–R); Cua and Heaton state that several pieces of prior information can be incorporated in this function (e.g. long-term

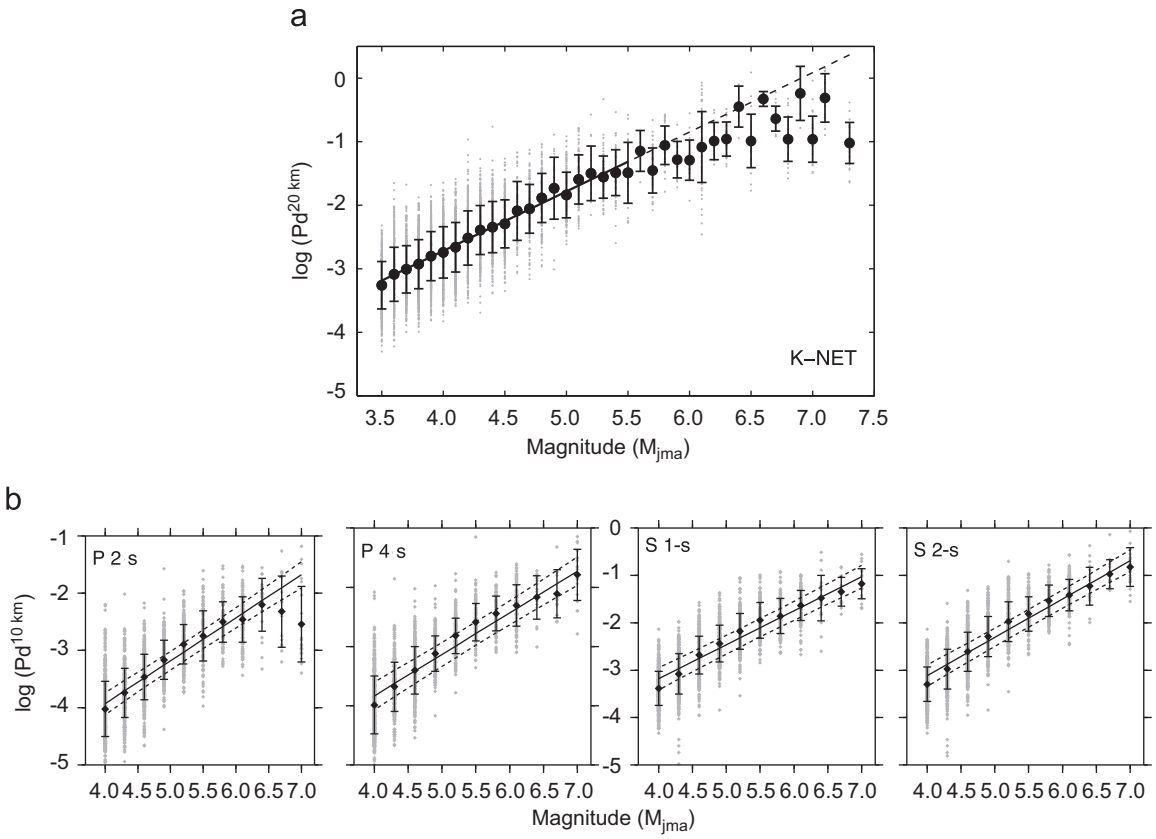

Fig. 6. (Top) Plot of the logarithm of the low-pass-filtered peak ground displacement P_d, normalized at a reference distance of 20 km, and the final magnitude, obtained by Rydelek et al. [51] using events recorded at the K–Net array in Japan and a window of 2-s after the *P* arrival. Black points represent the peak average on each magnitude bin with the associated standard deviation, while the grey dots are the peak values read on each record. The correlation is linear up to magnitude 5.5, but then it shows a saturation effect. (Bottom) Lancieri and Zollo [53] show, on a similar data set, that the saturation effect is removed by the use of larger time windows (4 s of *P*-wave) or using the peaks red on the *S*-waves. Here the peaks are normalized to a reference distance of 10 km.

national hazard maps, known fault traces, the G–R itself, for short-term forecast). In both papers, $f_{\mathbf{d}|M}(\mathbf{d}|m)$ is defined as a likelihood product, assuming that the observed data in **d** have a lognormal distribution and are statistically independent.

Lancieri and Zollo [53] further extended the above Bayesian approach by incorporating it into an *evolutionary* framework, where the magnitude PDF is updated at each time step after the event detection, as soon as new measurements are available. The *a priori* is initially set to the G–R relationship. Then, at every update, the prior information is given by the PDF retrieved at the previous step. Their approach makes use of the P_d parameter and takes into account for the previously mentioned saturation effect by assigning a constant probability for magnitudes larger than 6.5, when the 2*P* readings are used.

Another class of early warning parameters used for determining the earthquake size is constituted by integral measurements.

The EEW system in Istanbul [24] makes use of the cumulative absolute velocity (CAV) as a rapid detector for strong ground shaking. *CAV* is computed from the integral of the acceleration $a(t)$, and is defined as

$$CAV = \int_0^{t_{max}} |a(t)|\, dt \tag{10}$$

CAV is not strictly used for magnitude estimation, but, rather, to determine whether a damaging earthquake is occurring. When the *CAV* at given station exceeds a selectable first threshold, a trigger is set. The first alarm is declared upon verification of coincidence at three stations for the first *CAV* threshold. After the first alarm, a new, higher, threshold for *CAV* is set, and a second alert is notified when the new threshold is reached at 3 stations.

Festa et al. [54] introduced a similar measure, the integral of the squared velocity, or *IV*2, that is related to the early-radiated energy, and can be correlated with the magnitude. *IV*2 is defined as

$$IV2_c = \int_{t_c}^{t_c+\Delta t_c} v_c^2(t)\, dt \tag{11}$$

where the subscript c refers to the *P* or *S* phase, t_c is the corresponding first arrival, $v_c(t)$ is the particle velocity measured on the seismograms, and Δt_c is the length of the signal window on which the analysis is performed. Festa et al. investigated the scaling of *IV*2 with the final magnitude, over a large set of Japanese earthquakes, using time windows of 4*P* and 2*S*. They found that the energy (inferred from *IV*2) can predict the magnitude only for $M<5.8$, due to the limited segment of observed *P* or *S* signal. For $M>5.8$, the observed time window only provides a partial image of the advancing rupture, which comes from a fault portion that has almost the same area, despite the magnitude. However, by normalizing *IV*2 for the rupture area, the scaling with the magnitude is recovered in the full range $4<M<7$. They observe that the ratio between the squared peak displacement (P_d^2) and *IV*2 is a proxy for the initial slip and does not depend on the rupture area. Therefore, the scaling relationship between $\log(P_d^2/IV2)$ and magnitude can be used for early warning applications (Fig. 7). Furthermore, this quantity has the dimension of squared time and it is closely related to the τ_c parameter [55].

We complete this overview with the approach of Yamamoto et al. [56]. They introduced a new parameter, the seismic intensity magnitude M_I, which is defined from the instrumental seismic intensity I_p (in the JMA scale) measured on the *P*-wave:

$$M_I = I_p/2 + \log R + \pi f_p\, tt_p/(2.3Q_p) + b - c \tag{12}$$

where R is the hypocentral distance, tt_p, f_p and Q_p are respectively the travel time, the predominant frequency and the quality factor for the *P*-waves, b is a constant and c is a site correction term. The

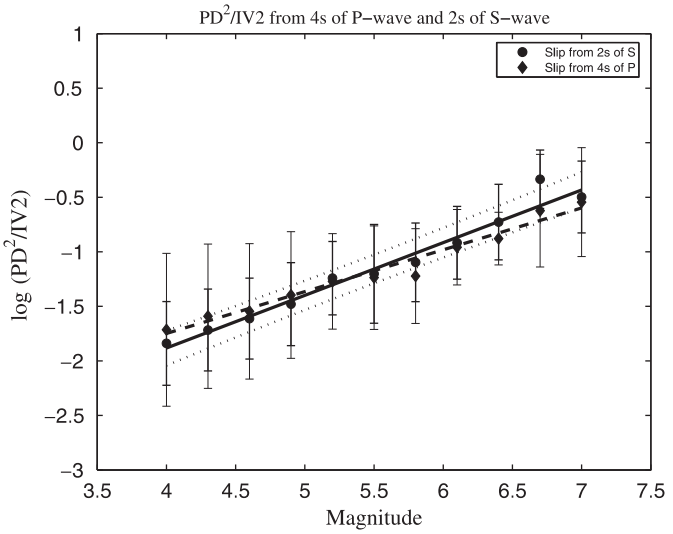

Fig. 7. Scaling of the ratio $PD^2/IV2$ as a function of the magnitude in the early portion of the *P*- and *S*-signal. The dotted lines represent the prediction bounds for a new observation with a 95% confidence level in correspondence of the *S* best-fit curve (from [54]).

observed seismic intensity I_p is defined as

$$I_p = 2\log V_a + 0.94 \tag{13}$$

where V_a is the level that the vector amplitude of the three-component acceleration (V) exceeds for more than 0.3 s, after the *P*-arrival. V_a can be measured in real-time and allows for quickly estimating the instrumental intensity I_p and the intensity magnitude M_I. Yamamoto et al. observed that M_I scales with M_w (as defined by JMA) up to $M_w=6.5$. The main advantage of the parameter V_a is however that it can be used to predict the instrumental intensity I_s, associated to *S*-waves, through an empirical relationship between I_p and I_s.

A synopsis of the parameters employed for rapid magnitude estimation is provided in Fig. 8, where they are categorized according to their physical interpretation and on the type of signal on which they are measured.

6.3. Physical models of the rupture process

Whether or not it is possible to determine the earthquake magnitude from the first few seconds of recorded signal rests on whether there are differences in the onsets of earthquakes of different sizes, which is ultimately controlled by the physics of the rupture process. The possible deterministic nature of earthquakes as inferred from the correlation of the initial *P*-wave amplitude and characteristic period and final magnitude has been largely investigated and debated in the recent literature [47,50–52,57,58].

The correlation between the initial *P*- and *S*-peak displacement amplitude and the final magnitude is explained in terms of basic earthquake source concepts [50,53,54]. Assuming that the peak ground displacement P_d depends on the relatively high frequency content of the signal, that the receivers are not in the immediate vicinity of the rupturing fault, and that the effect of rupture directivity and radiation pattern is averaged by the variable azimuthal position of the stations, the seismic radiation can be given in first approximation by the far-field effect of a point source. In this case the *P* and *S* displacement $u(t)$, at a given distance R, is expected to scale with moment rate $\dot{M}$ [59]:

$$u(t) = const\, \frac{1}{R}\dot{M}\left(t-\frac{R}{c}\right) = const\, \frac{1}{R}\Delta\dot{u}\ \Sigma = const\, \frac{1}{R}\Delta\dot{u}\, CL^2 \tag{14}$$

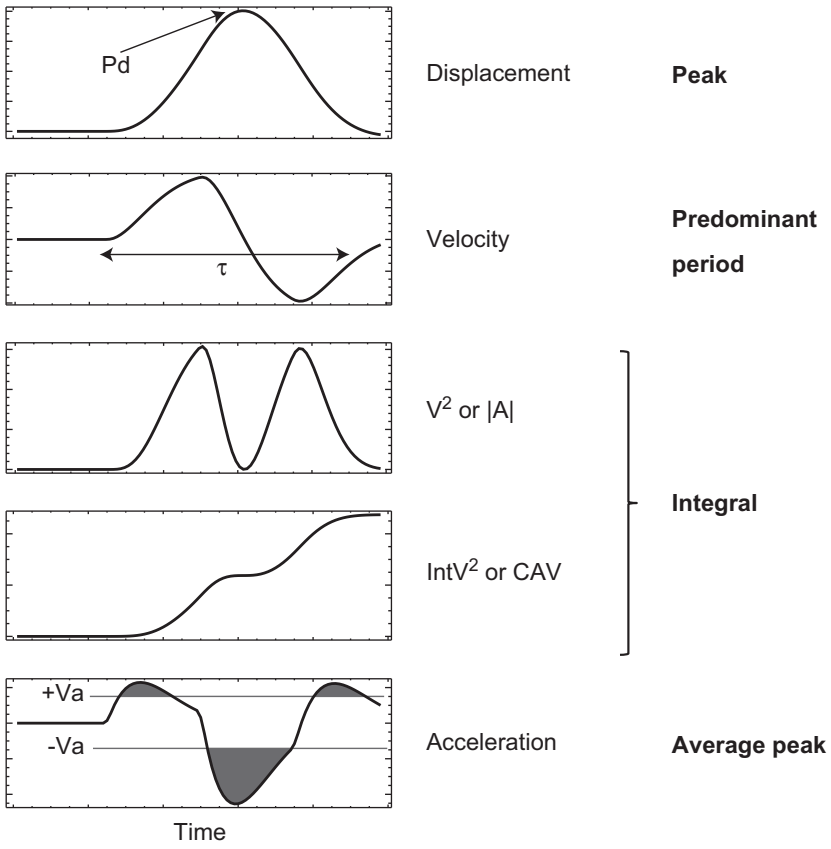

Fig. 8. The parameters used for real-time earthquake size determination can be subdivided into four groups: period parameters (e.g. τ_p and τ_c, mainly measured on velocity and displacement records, respectively), peak measurements (e.g. P_d, on displacement signals), integral quantities (e.g. *CAV* and *IV*2, measured on acceleration or velocity records) and peak levels (e.g. V_a, measured on the acceleration). See the text for the definition of each parameter.

where c is the wave velocity, $\Delta\dot{u}$ is the average slip velocity on the fault, Σ is the active fault area during the initial stage of the rupture, L a linear rupture dimension and C a geometrical factor of the order of 1. According to theoretical models of rupture dynamics [60,61], the slip rate amplitude, $\Delta\dot{u}$, scales linearly with dynamic stress drop $\Delta\sigma$.

On the other hand, the earthquake fracture development is controlled by the flow rate of elastic energy G [62,63]:

$$G = f\left(\frac{v_r}{\beta}\right)\frac{\Delta\sigma^2}{\mu}L \tag{15}$$

where f is a dimensionless function depending on fracture velocity v_r and loading conditions, and μ is the rigidity.

According to above theoretical results, both the far-field displacement $u(t)$ and the energy flux G depend on the stress-drop $\Delta\sigma$ and on the dimension of the fracture (through the parameter L). Since we expect that fractures with higher initial energy will have a greater possibility of propagating for long distances, the correlation between initial *P*- and *S*-peak displacements with magnitude therefore suggests that the final earthquake rupture size can be correlated to the initial stress-drop level and/or active slip area. Of course, this statement has to be taken only in a probabilistic (and not deterministic) sense, since the fracture propagation may also depend on the relative strength or weakness of the fault zones encountered.

These observations seem to contrast with the general view of the earthquake rupture occurring following a "cascade model" [64–66], where the rupture is assumed to start with a slip on a small fault patch and continues to grow along the fault plane as long as the conditions are favorable. This domino-type concept would imply that all earthquakes, large and small, begin in the same way from a small slip, and therefore the size of an earthquake cannot be determined until the entire rupture has run its course.

However several studies have pointed out the dependence of apparent and static stress release with seismic moment (e.g., [67–69]) in a wide seismic moment range, indicating that small and large event can be triggered at different stress release levels. Kanamori and Rivera [70], using a data set in a moment range of $10^{10} \leq \mathrm{Mo} \leq 10^{19}$ N m conclude that static stress drop and rupture velocity can scale differently for small and large earthquakes, and in particular stress drop could not necessarily be scale independent, although this scale independence is often implied.

On the other side, the hypothesis that the active-slip area Σ increases with magnitude would imply a dependence of slip duration (or rise-time) with magnitude. In interpreting the observed correlation between the predominant period parameter τ_p and magnitude, Olson and Allen [57] advanced the hypothesis that the predominant period is correlated to the slip duration in the early stages of the rupture. The scaling of τ_p with magnitude would therefore be evidence that the active-slip area depends on the earthquake size, even during the initial rupture phase.

The analysis of Japanese strong motion data has revealed the existence of a possible saturation effect on the initial *P*-peak displacement scaling with magnitude at about M 6.5, when measurements are performed in a 2 s time window after the first *P* arrival, while the saturation effect vanishes by enlarging the observation window to 3 or more seconds [51,52]. Interestingly, no saturation effect is observed (up to M about 7.5) on the

initial *S*-peak scaling relationship, even considering short time windows [53].

A possible explanation of the different scaling of *P* and *S* peaks with magnitude and of the saturation effect can be given using the concept of isochrone, defined as a curve of points on the fault plane whose radiation arrives at a given station at a given time *t* [71,72]. For a given time window after the first *P*- or *S*-arrivals, the isochrone encloses a portion of the fault area where the high frequency seismic radiation is emitted from. Let us note that, from the isochrone definition, it is expected that the rupture surface, where the first *X* seconds of *P* or *S* signals have been radiated from, is, in general, at least equal to, or bigger than, the fault surface which is expected to rupture in *X* seconds, depending on the position of the observer relative to the fault plane. Moreover, as the *S* waves are slower than *P* waves, the surface imaged by the *S* isochrones of *X* seconds of duration will be much larger than by *P* waves in the same time window [53].

In a very recent work, Murphy and Nielsen [73] argue that for magnitude below the observed saturation threshold (*M* 6.5), the average area imaged by the 2-s, *P* isochrones is larger or comparable with the final fault size, thus explaining the observed correlation between *PD* and magnitude. This suggests that for higher magnitude values the saturation effect is due to an under-sampling of the fault plane, when 2 s of *P* signal are used. Extending the *P* window to 4 s, or using 2 s of *S* window, larger fault surfaces are sampled, and the scaling extends up to *M* about 7.5, consistently with observations from Japanese strong motion data [53]. However, for larger magnitude events the saturation effect can be dominant so to make the magnitude unpredictable using only a small portion of the initial *P*- and *S*-wave recorded signal.

6.4. Shaking intensity estimation

Strength of shaking can practically be represented by peak ground acceleration (PGA) and peak ground velocity (PGV). For regional EEW approach, the shaking intensity estimation is a relatively easy problem. As soon as the EEW system provides an estimate of earthquake location and magnitude, the expected PGA and PGV at a certain target can be evaluated through the use of standard attenuation relationships of peak ground motions and site factors for the selected target site. Most of the regional EEW techniques use this approach [18,74–76]. The estimated values of PGA and PGV can then be transposed, using a regression relationship, into a scale of instrumental intensity (e.g. [77,78]) and represented as ground shaking maps ([79,29]; Fig. 9).

On the contrary, onsite EEW systems generally follow a different strategy that does not require the estimation of earthquake location and magnitude (though some approaches also evaluate source parameters, e.g. [17,39]). Onsite EEW methods take advantage of the different velocity of propagation of *P*- and *S*-waves, using the information carried from the former to rapidly predict the peak ground motion determined at the site by the latter.

Wu and Kanamori [41] showed that the maximum amplitude of a high-pass filtered vertical displacement, measured on the initial 3 s of the *P*-wave (namely P_d) can be used to estimate the

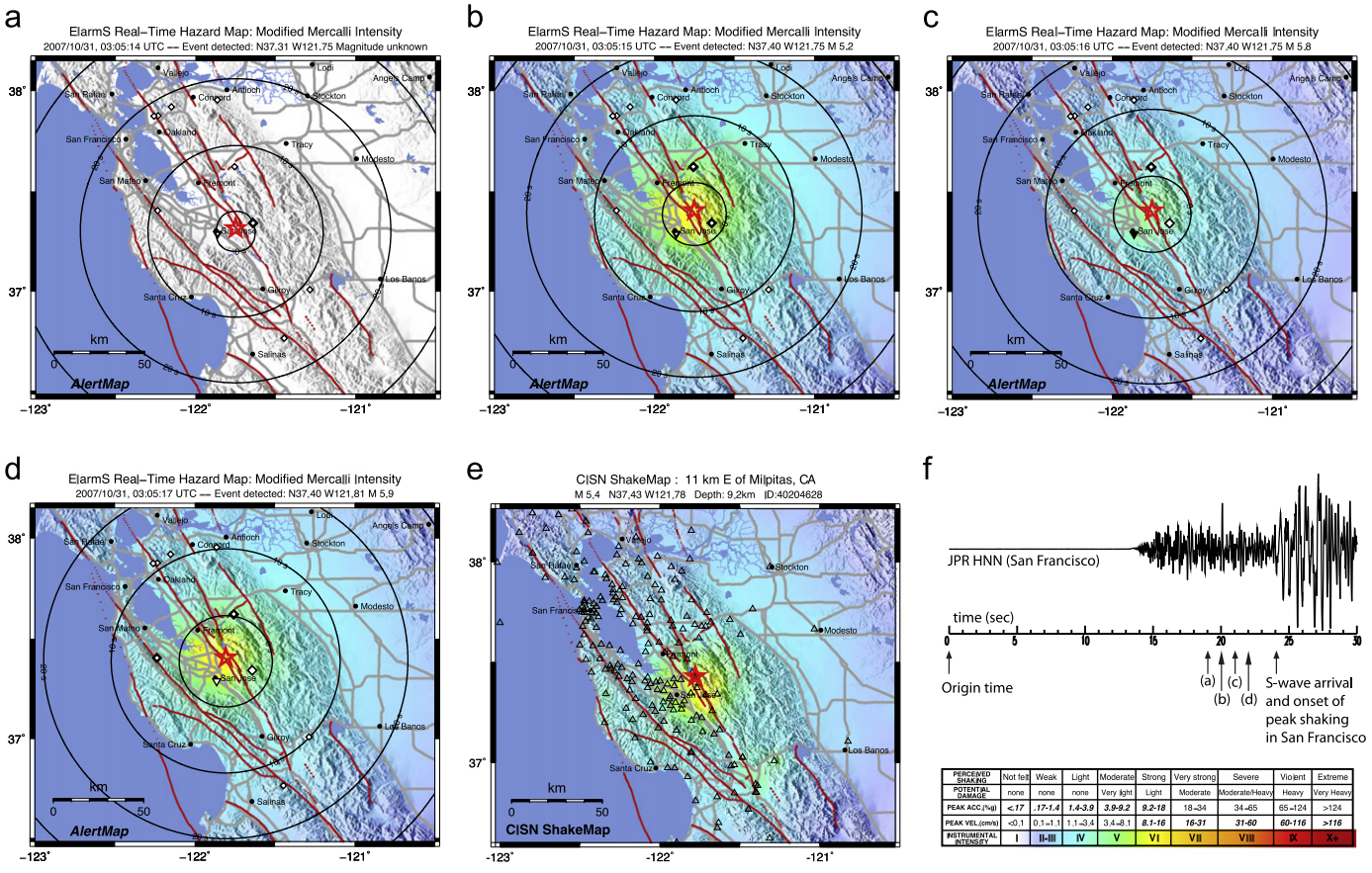

Fig. 9. Example of ElarmS AlertMaps for a M_w 5.4 earthquake in the San Francisco Bay Area. (a–d) AlertMaps generated 19, 20, 21 and 22 s after the origin time. Seismic stations are normally white and grey when they have detected a *P*-wave trigger, black during the period of expected peak ground shaking, and colored according to the MMI scale once peak shaking has been observed. The star shows the earthquake location and the circles are the estimated warning time. Faults are indicated in red and major roads are grey. (e) CISN ShakeMap published after the event. (f) Timeline comparing the AlertMap availability with the arrival of peak ground shaking in San Francisco. (From Brown et al. [87]).

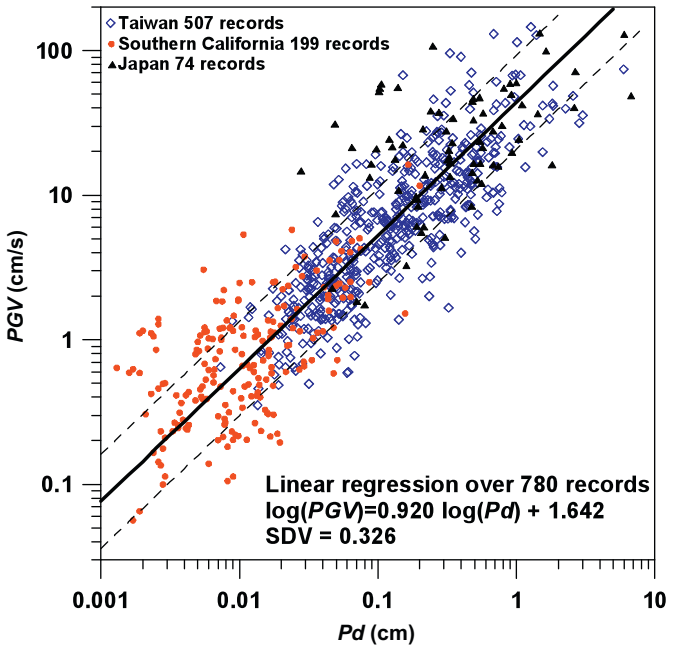

Fig. 10. Relationship between peak initial displacement amplitude (P_d) measurements and peak ground velocity (*PGV*) for the records with epicentral distances less than 30 km from the epicenter in Southern California (red solid circles), Taiwan (blue diamonds) and Japan (black solid triangles). Solid line shows the least squares fit and the two dashed lines show the range of one standard deviation (from [44]). (For interpretation of the references to colour in this figure legend, the reader is referred to the web version of this article.)

Table 2
Decision table for an onsite EEW system based on the use of the early peak ground displacement P_d and the period parameter τ_c [43].

P_d (cm)	τ_c (s)	Warning type
>0.5	>1.0	The event is most likely damaging in the station area as well as a larger area.
<0.5	>1.0	The event is not damaging in the station area, but it can be damaging in other areas.
>0.5	<1.0	The event is damaging only in a limited area around the station.
<0.5	<1.0	The event is not damaging.

PGV at the same site. By analyzing 780 traces, with epicentral distances less than 30 km, recorded in Japan, Taiwan and southern California (Fig. 10, [44]), they verified that $\log PGV$ and $\log P_d$ follow a relationship of the form:

$$\log PGV = A \log P_d + B \tag{16}$$

where A and B are to be determined by a regression analysis.

Relation (16) provides a mean to predict the PGV carried by *S*-waves, based on a measurement performed on the first seconds of *P*-waves. Nevertheless, that relation does not depend on magnitude, in the sense that the same values of P_d (and thus of PGV) could be due to a moderate but close earthquake or to a large, distant event. The authors proposed to combine the P_d parameter with the τ_c parameter, which scales with the magnitude [9], into a single indicator. They observed that the product $P_d\tau_c$ is a clear benchmark for discriminating damaging from non-damaging events. In particular, for the network geometry of Taiwan, a value of $P_d\tau_c \geq 1.0$ cm indicates a most likely damaging earthquake. As an alternative, P_d and τ_c can be used separately for constructing a decision rule (Table 2).

Also for the onsite approach, the predicted peak ground shaking can be used to determine the expected intensity, through a regression relationship. Wu and Kanamori [44] argued that the shaking intensity can be estimated from a single station with a standard deviation of 1.0 unit of MMI scale or 0.6 units of Japan and Taiwan intensity scale.

7. Summary and discussion

With more than 20 years of developments, earthquake early warning (EEW) is today becoming an effective answer to the problem of seismic risk mitigation at short time-scales. A few countries worldwide have operative systems, while several others are actively experimenting and prototyping.

Today there are no strong objections to the possibility of developing and implementing EEW systems. The United Nations have recently promoted early warning, and associated preparedness and response systems, as the most effective strategy for the mitigation of diverse natural hazards [80], and have provided guidelines for the implementation and the deployment of such systems, through the International Strategy for Disaster Reduction [81].

However, the debate within the scientific community is still ongoing, and is today primarily focused on the following key topics: (1) What is the accuracy and the reliability of the different parameters employed for the prediction of the earthquake size? (2) Do the empirical relationships between these parameters and the earthquake size really saturate for larger events (M 6–7), implying that larger magnitudes cannot be correctly predicted? (3) Which is the best approach to follow between the onsite and the regional?

Concerning the first question, several efforts are ongoing in assessing and comparing the performances of different EEW methodologies. The California Integrated Seismic Network (CISN) has recently developed an infrastructure that allows for testing EEW algorithms in a real-time environment, with the objective to evaluate the rapidity and the accuracy of each methodology and to compare the resulting warning messages [82–84]. Recently, Zollo et al. [76] presented an extensive synthetic test of regional EEW in Southern Italy, and introduced three quantitative parameters to assess the system performances.

The second issue is probably more theoretical than practical. Do we really need to know the actual magnitude, if $M \geq 6.5$, before issuing an alert? Within the epicentral area ($\sim$50 km of radius), a shallow earthquake with $M \geq 6.5$ is likely to produce damage in any case. For distant targets the trade-off between the risk of under-estimating the damages and the lead-time can be handled by each application, according to the required level of confidence.

Finally, the choice of the most appropriate approach to EEW (regional, on-site, or mixed) has to be based on the knowledge of the target area: the distribution of seismogenic zones, the type of seismicity (depth, mechanism, magnitude range) and the site characteristics. The onsite approach has faster report times, close to the epicenter, and generally produces robust estimates of the local ground shaking, but, typically, the earthquake source parameters are poorly determined; the regional approach is slower at small epicentral distances, but it can provide accurate estimates of location and magnitude, though the quality of the ground motion prediction depends on the accuracy of the employed attenuation relationship. In the last years the two approaches started to converge. The Japanese regional EEW system integrates an onsite approach in order to reduce reporting times and provide warnings to sites close to the epicentral area [18]. Moreover, new methods for earthquake detection and location, designed for the regional approach, can provide information with one single triggering station [30,35].

The effectiveness of an EEW system is however not only related to the performances and the accuracy of the methodologies employed. Other parameters play a crucial role and should be part of the design process of the system.

EEW applications should be aware of the trade-off between time and accuracy, and they should include real-time strategies for the reduction of the vulnerability and/or the exposure (e.g. [13]). The JMA experience in Japan [85] shows that this can (and should) be done both at a general level (by developing strategies to protect public officials, key safety personnel and the public), and at the end-user level (factories, power plants, other facilities), where the JMA broadcast is integrated with local systems that can include site-specific EEW procedures.

Last, but not least, the success of an EEW system is strictly connected to the education and the awareness of the general public and the end-users. It is necessary that local management policies, education and training of the population, and the understanding of the costs related to missed- or false alarms enter, as a final component, into the development of a really effective EEW system.

Acknowledgements

This research was supported by the Italian DPC-S5 project and by the National Science Council of the Republic of China. This work was partially funded by AMRA scarl through the EU-SAFER project (Contract 036935). We thank Maria Lancieri for useful discussion and helpful comments.

References

[1] Kanamori H, Hauksson E, Heaton TH. Real-time seismology and earthquake hazard mitigation. Nature 1997;390:461–4, doi:10.1038/37280.
[2] Snieder R, van Eck T. Earthquake prediction: a political problem? International Journal of Earth Sciences 1997;86:446–63.
[3] Kanamori H. Earthquake prediction: an overview. In: Lee WHK, Kanamori H, Jennings PC, Kisslinger C, editors. International handbook of earthquake and engineering seismology, Part B. Amsterdam. ISBN: 978-0-12-440658-2. p. 1205–16.
[4] Kanamori H. Earthquake physics and real-time seismology. Nature 2008;451:271–3, doi:10.1038/nature06585.
[5] Heaton TA. Model for a seismic computerized alert network. Science 1985;228(4702):987–90, doi:10.1126/science.228.4702.987.
[6] United States National Research Council. Real-time earthquake monitoring. Report from the Committee on Seismology. Washington, DC, USA: National Academy Press; 1991 52 pp.
[7] United States Geological Survey. A plan for implementing a real-time seismic hazard warning system. A report to congress required by public law 105-47, March 24, 1998, USA, 1998.
[8] Lee WHK, Espinosa-Aranda JM. Earthquake early warning systems: current status and perspectives. In: Zschau J, Kuppers AN, editors. Early warning systems for natural disaster reduction. Berlin. ISBN: 3-540-67962-6. p. 409–23.
[9] Kanamori H. Real-time seismology and earthquake damage mitigation. Ann Rev Earth Planet Sci 2005;33:195–214, doi:10.1146/annurev.earth.33.092203.122626.
[10] Gasparini P, Manfredi G, Zschau J, editors. Earthquake early warning systems. Berlin. ISBN: 978-3-540-72240-3 350 pp.
[11] Allen RM, Gasparini P, Kamigaichi O, Böse M. The status of earthquake early warning around the world: an introductory overview. Seismol Res Lett 2009;80(5):682–93, doi:10.1785/gssrl.80.5.682.
[12] Cooper JD. Letter to editor. San Francisco Daily Evening Bulletin, November 3, 1868.
[13] Iervolino I, Convertito V, Giorgio M, Manfredi G, Zollo A. Real-time risk analysis for hybrid earthquake early warning systems. J Earthquake Eng 2006;10(6):867–85, doi:10.1142/S1363246906002955.
[14] Iervolino I, Giorgio M, Galasso C, Manfredi G. Uncertainty in early warning predictions of engineering ground motion parameters: What really matters? Geophys Res Lett 2009;36:L00B06 doi:10.1029/2008GL036644.
[15] Espinosa-Aranda J, Jiménez A, Ibarrola G, Alcantar F, Aguilar A, Inostroza M, et al. Mexico City seismic alert system. Seism Res Lett 1995;66(6):42–53.
[16] Suarez G, Novelo D, Mansilla E. Performance evaluation of the seismic alert system (SAS) in Mexico City: a seismological and a social perspective. Seismol Res Lett 2009;80(5):707–16, doi:10.1785/gssrl.80.5.707.
[17] Odaka T, Ashiya K, Tsukada S, Sato S, Ohtake K, Nozaka D. A new method of quickly estimating epicentral distance and magnitude from a single seismic record. Bull Seism Soc Am 2003;93:526–32, doi:10.1785/0120020008.
[18] Kamigaichi O. JMA earthquake early warning. J Jpn Assoc Earthquake Eng 2004;4(3):134–7.
[19] Wu YM, Teng TL. A virtual sub-network approach to earthquake early warning. Bull Seism Soc Am 2002;92(5):2008–18, doi:10.1785/0120010217.
[20] Wu YM, Hsiao NC, Lee WHK, Teng TL, Shin TC. State of the art and progress in the earthquake early warning system in Taiwan. In: Gasparini P, Manfredi G, Zschau J, editors. Earthquake early warning systems. Berlin: Springer; 2007. p. 283–306, doi:10.1007/978-3-540-72241-0_14.
[21] Hsiao NC, Wu YM, Shin TC, Zhao L, Teng TL. Development of earthquake early warning system in Taiwan. Geophys Res Lett 2009;36:L00B02, doi:10.1029/2008GL036596.
[22] Wenzel F, Oncescu M, Baur M, Fiedrich F. An early warning system for Bucharest. Seismol Res Lett 1999;70(2):161–9.
[23] Böse M, Ionescu C, Wenzel F. Earthquake early warning for Bucharest, Romania: novel and revised scaling relations. Geophys Res Lett 2007;34:L07302, doi:10.1029/2007GL029396.
[24] Erdik M, Fahjan Y, Ozel O, Alcik H, Mert A, Gul M. Istanbul earthquake rapid response and the early warning system. Bull Earthquake Eng 2003;1(1):157–63, doi:10.1023/A:1024813612271.
[25] Böse M, Wenzel F, Erdik M. PreSEIS: a neural network based approach to earthquake early warning for finite faults. Bull Seism Soc Am 2008;98(1):366–82, doi:10.1785/0120070002.
[26] Alcik H, Ozel O, Apaydin N, Erdik M. A study on warning algorithms for Istanbul earthquake early warning system. Geophys Res Lett 2009;36:L00B05, doi:10.1029/2008GL036659.
[27] Allen RM, Kanamori H. The potential for earthquake early warning in Southern California. Science 2003;300:786–9, doi:10.1126/science.1080912.
[28] Wurman G, Allen RM, Lombard P. Toward earthquake early warning in Northern California. J Geophys Res 2007;112:B08311, doi:10.1029/2006JB004830.
[29] Allen RM, Brown H, Hellweg M, Khainovski O, Lombard P, Neuhauser D. Real-time earthquake detection and hazard assessment by ElarmS across California. Geophys Res Lett 2009;36:L00B08, doi:10.1029/2008GL036766.
[30] Cua G, Heaton T. The Virtual Seismologist (VS) method: a Bayesian approach to earthquake early warning. In: Gasparini P, Manfredi G, Zschau J, editors. Earthquake early warning systems. Berlin: Springer; 2007. p. 97–132, doi:10.1007/978-3-540-72241-0_7.
[31] Iannaccone G, Zollo A, Elia L, Convertito V, Satriano C, Martino C, et al. A prototype system for earthquake early-warning and alert management in southern Italy. Bull Earthquake Eng 2009, 10.1007/s10518-009-9131-8.
[32] Allen R. Automatic earthquake recognition and timing from single traces. Bull Seismol Soc Am 1978;68(5):1521–32.
[33] Rydelek P, Pujol J. Real-time seismic warning with a two-station subarray. Bull Seismol Soc Am 2004;94(4):1546–50, doi:10.1785/012003197.
[34] Horiuchi S, Negishi H, Abe K, Kamimura A, Fujinawa Y. An automatic processing system for broadcasting earthquake alarms. Bull Seism Soc Am 2005;95:708–18, doi:10.1785/0120030133.
[35] Satriano C, Lomax A, Zollo A. Real-time evolutionary earthquake location for seismic early warning. Bull Seism Soc Am 2008;98(3):1482–94, doi:10.1785/0120060159.
[36] Font Y, Kao H, Lallemand S, Liu CS, Chiao LY. Hypocentral determination offshore eastern Taiwan using the maximum intersection method. Geophys J Int 2004;158:655–75, doi:10.1111/j.1365-246X.2004.02317.x.
[37] Rosenberger A. Arrival-time order location revisited. Bull Seismol Soc Am 2009;99(3):2027–34, doi:10.1785/0120080270.
[38] Satriano C, Elia L, Martino C, Lancieri M, Zollo A, Iannaccone G. PRESTo, the earthquake early warning system for Southern Italy: concepts, capabilities and future perspectives. Soil Dyn Earthquake Eng 2010, doi:10.1016/j.soildyn.2010.06.008.
[39] Nakamura Y. On the urgent earthquake detection and alarm system (UrEDAS). In: Proceedings of ninth world conference on earthquake engineering, Tokyo–Kyoto, Japan, 1988.
[40] Nakamura Y. Development of the earthquake early-warning system for the Shinkansen, some recent earthquake engineering research and practical in Japan. The Japanese National Committee of the International Association for Earthquake Engineering 1984:224–38.
[41] Wu YM, Kanamori H. Exploring the feasibility of on-site earthquake early warning using close-in records of the 2007 Noto Hanto earthquake. Earth Planets and Space 2008;60:155–60.
[42] Wu YM, Kanamori H. Experiment on an onsite early warning method for the Taiwan early warning system. Bull Seism Soc Am 2005;95(1):347–53, doi:10.1785/0120040097.
[43] Wu YM, Kanamori H. Rapid assessment of damaging potential of earthquakes in Taiwan from the beginning of *P* waves. Bull Seism Soc Am 2005;95(3):1181–5, doi:10.1785/0120040193.
[44] Wu YM, Kanamori H. Development of an earthquake early warning system using real-time strong motion signals. Sensors 2008;8(1):1–9, doi:10.3390/s8010001.
[45] Wu YM, Yen HY, Zhao L, Huang BS, Liang WT. Magnitude determination using initial *P* waves: a single-station approach. Geophys Res Lett 2006;33:L05306, doi:10.1029/2005GL025395.

[46] Wu YM, Kanamori H, Allen RM, Hauksson E. Determination of earthquake early warning parameters, τ_c and P_d, for southern California. Geophys J Int 2007;170(2):711–7, doi:10.1111/j.1365-246X.2007.03430.x.
[47] Rydelek P, Horiuchi S. Is earthquake rupture deterministic?Nature 2006;442:E5–6 doi:10.1038/nature04963.
[48] Yamada T, Ide S. Limitation of the predominant-period estimator for earthquake early warning and the initial rupture of earthquakes. Bull Seism Soc Am 2008;98(6):2739–45, doi:10.1785/0120080144.
[49] Wu YM, Zhao L. Magnitude estimation using the first three seconds *P*-wave amplitude in earthquake early warning. Geophys Res Lett 2006;33:L16312, doi:10.1029/2006GL026871.
[50] Zollo A, Lancieri M, Nielsen S. Earthquake magnitude estimation from peak amplitudes of very early seismic signals on strong motion records. Geophys Res Lett 2006;33:L23312, doi:10.1029/2006GL027795.
[51] Rydelek P, Wu C, Horiuchi S. Comment on "Earthquake magnitude estimation from peak amplitudes of very early seismic signals on strong motion records" by Aldo Zollo, Maria Lancieri, and Stefan Nielsen. Geophys Res Lett 2007;34:L20302, doi:10.1029/2007GL029387.
[52] Zollo A, Lancieri M, Nielsen S. Reply to comment by P. Rydelek et al. on "Earthquake magnitude estimation from peak amplitudes of very early seismic signals on strong motion records". Geophys Res Lett 2007;34:L20303, doi:10.1029/2007GL030560.
[53] Lancieri M, Zollo A. A Bayesian approach to the real-time estimation of magnitude from the early *P* and *S* wave displacement peaks. J Geophys Res 2008;113:B12302, doi:10.1029/2007JB005386.
[54] Festa G, Zollo A, Lancieri M. Earthquake magnitude estimation from early radiated energy. Geophys Res Lett 2008;35(22):L22307, doi:10.1029/2008GL035576.
[55] Festa G, Zollo A. Early radiation and final magnitude: insights from source kinematics. In: Proceedings of the second EEW workshop in Kyoto. JSPS/DPRI, 2009 .
[56] Yamamoto S, Rydelek P, Horiuchi S, Wu C, Nakamura H. On the estimation of seismic intensity in earthquake early warning systems. Geophys Res Lett 2008;35(7):L07302, doi:10.1029/2007GL033034.
[57] Olson EL, Allen RM. The deterministic nature of earthquake rupture. Nature 2005;438:212–5, doi:10.1038/nature04214.
[58] Hellemans A. Do early tremors give sneak preview of Quake's power? Science 2006;314(5806):1670, doi:10.1126/science.314.5806.1670.
[59] Aki K, Richards P. Quantitative seismology. 2nd ed. University Science Books; 978-0935702965 704 pp.
[60] Kostrov BV. Self-similar problems of propagation of shear cracks. J Appl Math Mech 1964;28(5):1077–87.
[61] Scholz CH. The mechanics of earthquakes and faulting. 2nd ed.. New York: Cambridge University Press; 9780521655408 496 pp.
[62] Broberg KB. Cracks and fracture. London: Academic Press; 978-0-12-134130-5 752 pp.
[63] Nielsen S. Can earthquake size be controlled by the initial seconds of rupture? In: Gasparini P, Manfredi G, Zschau J, editors. Earthquake early warning systems. Berlin: Springer; 2007. p. 9–20, doi:10.1007/978-3-540-72241-0_2.
[64] Brune JN. Implications of earthquake triggering and rupture propagation for earthquake prediction based on premonitory phenomena. J Geophys Res 1979;84:2195–8, doi:10.1029/JB084iB05p02195.
[65] Ellsworth WL, Beroza GC. Seismic evidence for an earthquake nucleation phase. Science 1995;268:851–5, doi:10.1126/science.268.5212.851.
[66] Ellsworth WL, Beroza GC. Observation of the seismic nucleation phase in the Ridgecrest, California, earthquake sequence. Geophys Res Lett 1998;25:401–4.
[67] De Natale G, Madariaga R, Scarpa R, Zollo A. Source parameter analysis from strong motion records of the Friuli, Italy, earthquake sequence (1976–1977). Bull Seism Soc Am 1987;77:1127–46.
[68] Kanamori H, Heaton TH. Microscopic and macroscopic physics of earthquakes. Geophys Monograph 2000;120:147–63.
[69] Beeler NM, Wong TF, Hickman SH. On the expected relationships among apparent stress, static stress drop, effective shear fracture energy, and efficiency. Bull Seismol Soc Am 2003;93(3):1381–9, doi:10.1785/0120020162.
[70] Kanamori H, Rivera L. Static and dynamic scaling relations for earthquakes and their implications for rupture speed and stress drop. Bull Seism Soc Am 2004;94(1):314–9, doi:10.1785/0120030159.
[71] Spudich P, Frazer N. Use of ray theory to calculate high-frequency radiation from earthquake sources having spatially variable rupture velocity and stress drop. Bull Seism Soc Am 1984;74(6):2061–82.
[72] Bernard P, Madariaga R. High-frequency seismic radiation from a buried circular fault. Geophys J Roy Astron Soc 1984;78(1):1–17, doi:10.1111/j.1365-246X.1984.tb06468.x.
[73] Murphy S, Nielsen S. Estimating earthquake magnitude with early arrivals: a test using dynamic and kinematic models. Bull Seismol Soc Am 2009;99(1):1–23, doi:10.1785/0120070246.
[74] Wu YM, Shin TC, Chang CH. Near real-time mapping of peak ground acceleration and peak ground velocity following a strong earthquake. Bull Seism Soc Am 2001;91:1218–28, doi:10.1785/0120000734.
[75] Allen RM. The ElarmS earthquake early warning methodology and its application across California. In: Gasparini P, Manfredi G, Zschau J, editors. Earthquake early warning systems. Berlin: Springer; 2007. p. 21–43, doi:10.1007/978-3-540-72241-0_3.
[76] Zollo A, Iannaccone G, Lancieri M, Cantore L, Convertito V, Emolo A, et al. Earthquake early warning system in southern Italy: methodologies and performance evaluation. Geophys Res Lett 2009;36:L00B07, doi:10.1029/2008GL036689.
[77] Wald DJ, Quitoriano V, Heaton TH, Kanamori H. Relationships between peak ground acceleration, peak ground velocity, and modified Mercalli intensity in California. Earthquake Spectra 1999;15(3):557–64, doi:10.1193/1.1586058.
[78] Wu YM, Teng TL, Shin TC, Hsiao NC. Relationship between peak ground acceleration, peak ground velocity, and intensity in Taiwan. Bull Seism Soc Am 2003;93(1):386–96, doi:10.1785/0120020097.
[79] Wald DJ, Quitoriano V, Heaton TH, Kanamori H, Scrivner CW, Worden CB. TriNet "ShakeMaps": rapid generation of peak ground motion and intensity maps for earthquakes in Southern California. Earthquake Spectra 1999;15(3):537–55, doi:10.1193/1.1586057.
[80] United Nations. Global Survey of Early Warning Systems—an assessment of capacities, gaps and opportunities toward building a comprehensive global early warning system for all natural hazards. A report prepared at the request of the Secretary-General of the United Nations, 2006.
[81] International Strategy for Disaster Reduction. 〈http://www.unisdr.org/〉, last visited June 2010.
[82] Solanki K, Hauksson E, Kanamori H, Friberg P, Wu YM. Implementation of real-time testing of earthquake early warning algorithms: using the California Integrated Seismic Network (CISN) infrastructure as a test bed for the *P* amplitude and period monitor for a single station. Eos Trans. AGU 2006;87(52) Fall Meet Suppl, Abstract S31A-0175.
[83] Böse M, Hauksson E, Solanki K, Kanamori H, Heaton TH, Wu YM. Real-time testing of on-site earthquake early warning within the California Integrated Seismic Network (CISN) using statewide distributed and on-site processing. Eos Trans AGU 2008;89(53) Fall Meet Suppl, Abstract S11-1727.
[84] Cua G, Maechling P. Evaluating and comparing performance of earthquake early warning algorithms. Geophys Res Abstracts 2008;10. EGU2008-A-06753.
[85] Kamigaichi O, Saito M, Doi K, Matsumori T, Tsukada S, Takeda K, et al. Earthquake early warning in Japan: warning the general public and future prospects. Seismol Res Lett 2009;80(5):717–26, doi:10.1785/gssrl.80.5.717.
[86] Horiuchi S, Horiuchi Y, Yamamoto S, Nakamura H, Wu C, Rydelek PA, Kachi M. Home seismometer for earthquake early warning. Geophys Res Lett 2009;36:L00B04, doi:10.1029/2008GL036572.
[87] Brown HM, Allen RM, Hellweg M, Khainovski O, Neuhauser D, Souf A. Development of the ElarmS methodology for earthquake early warning: realtime application in California and offline testing in Japan. Soil Dyn Earthquake Eng 2010, doi:10.1016/j.soildyn.2010.03.008.